Physics of Fluids

RESEARCH ARTICLE | JANUARY 16 2026

An integrated computational workflow for myocardial perfusion combining the multiple-network poroelastic theory and subject-specific imaging data

Xingyu Su (苏星宇); Zeyan Li (李泽燕); Xin Yuan (袁昕); Yuting Yang (杨钰婷); Liwei Guo (郭立伟); Duanduan Chen (陈端端)

Check for updates

Physics of Fluids 38, 011911 (2026)
https://doi.org/10.1063/5.0300204

View Online
Export Citation

Articles You May Be Interested In

Stenosis severity and heart rate effects on left coronary artery hemodynamics and myocardial oxygen balance: A comprehensive assessment using pressure gradient

Physics of Fluids (February 2024)

Computational modeling of gelation of hydrogel for myocardial infarction therapy in rat myocardium: Capturing non-linear losses using time-dependent viscosity

Physics of Fluids (November 2025)

An open loop 0D-3D modeling of pulsatile hemodynamics for the diagnosis of a suspected coronary arterial disease with patient data

Physics of Fluids (October 2023)

16 January 2026 16:04:00

AIP Publishing

AIP Advances
Why Publish With Us?
21DAYS average time to 1st decision
OVER 4 MILLION views in the last year
INCLUSIVE scope
Learn More
AIP Publishing

An integrated computational workflow for myocardial perfusion combining the multiple-network poroelastic theory and subject-specific imaging data

Cite as: Phys. Fluids **38**, 011911 (2026); doi: 10.1063/5.0300204
Submitted: 31 August 2025 · Accepted: 22 December 2025 ·
Published Online: 16 January 2026

View Online Export Citation CrossMark

Xingyu Su (苏星宇),[1] Zeyan Li (李泽燕),[1,2] Xin Yuan (袁昕),[3,4] Yuting Yang (杨钰婷),[1] Liwei Guo (郭立伟),[5,a)] and Duanduan Chen (陈端端)[1,a)]

AFFILIATIONS

[1] School of Medical Technology, Beijing Institute of Technology, Beijing 100081, China
[2] Department of Psychiatry, The Chinese University of Hong Kong, Hong Kong SAR 999077, China
[3] State Key Laboratory of Cardiovascular Disease, Fuwai Hospital, National Centre for Cardiovascular Diseases, Chinese Academy of Medical Sciences and Peking Union Medical College, Beijing 100037, China
[4] Department of Cardiac Surgery, Fuwai Hospital, Chinese Academy of Medical Sciences and Peking Union Medical College, Beijing 100037, China
[5] Department of Mechanical Engineering, University College London, London WC1E 7JE, United Kingdom

a) Authors to whom correspondence should be addressed: liwei.guo@ucl.ac.uk and duanduan@bit.edu.cn

ABSTRACT

Microvascular dysfunction plays an early and potentially independent role in coronary artery disease, yet remains difficult to assess due to limitations in current imaging resolutions and diagnostic tools. To address this gap, we present an integrated computational workflow for subject-specific myocardial perfusion modeling based on the multiple-network poroelastic theory (MPET). The myocardium is represented as a poroelastic medium containing three interacting fluid networks: arterial, arteriole/capillary, and venous, to capture the multiscale dynamics of myocardial perfusion. Specifically, the workflow integrates realistic left ventricular morphology and physiologically informed coronary inflow patterns derived from routine magnetic resonance (MR) imaging into the MPET framework. Sensitivity analysis guided parameter calibration to ensure physiological relevance of the myocardial perfusion model. The simulation results showed that the model reproduced physiologically realistic myocardial blood flow patterns and transmural perfusion gradients, in agreement with clinical MR perfusion imaging. Notably, the model demonstrated sensitivity to myocardial wall thickness, highlighting its potential for assessing structural–functional relationships.

© *2026 Author(s). All article content, except where otherwise noted, is licensed under a Creative Commons Attribution (CC BY) license (https://creativecommons.org/licenses/by/4.0/).* https://doi.org/10.1063/5.0300204

I. INTRODUCTION

Myocardial perfusion is the process by which oxygen and nutrients are delivered to cardiac tissue through the coronary microvasculature. Perfusion impairment is a key manifestation of coronary artery disease (CAD), and increasing evidence suggests that microvascular dysfunction may precede and even occur independently of epicardial coronary stenosis.[1] However, compared with the extensively studied epicardial coronary arteries, current methods for assessing microvascular function remain limited.[2] Myocardial blood flow (MBF) is a key quantitative indicator of perfusion, commonly assessed using positron emission tomography (PET), computed tomography (CT), or cardiovascular magnetic resonance (CMR) perfusion imaging. Despite their routine clinical use, these imaging modalities remain limited in accurately characterizing microvascular function due to low spatial resolution, elevated scanning cost, and reliance on contrast agents.

Computational models can provide a flexible framework for simulating myocardial perfusion in different physiological and pathological scenarios, which can be used as virtual diagnostic and treatment planning tools. However, coronary perfusion spans more than four orders of magnitude in spatial scale, and microvessels with diameters

16 January 2026 16:04:00

less than 200 μm constitute more than 95% of the vascular network.[3] Explicit vascular modeling is constrained by both anatomical data availability and computational cost.[4] Therefore, homogenized porous media models provide a practical and physiologically justified strategy for myocardial perfusion modeling.

Terzaghi[5] and Biot[6] first described the mechanical behavior of porous media using the elastic theory and Darcy's law. Earlier modeling of myocardium typically idealized the left ventricle as an axisymmetric structure[7–11] whereas representing the coronary vasculature using a single compartment.[8–10] However, coronary flow exhibits distinct behaviors across different scales, which single-compartment models fail to capture adequately. One strategy addresses this by generating vascular structures from imaging or algorithmic approaches, which are solved using 1D or 3D fluid dynamics equations and coupled with homogenized capillary models to simulate multiscale myocardial perfusion.[12–15] Alternatively, multicompartment models have been employed to capture scale-specific flow dynamics.[4,16,17] Both approaches emphasize the increasing need for anatomically accurate and physiologically realistic modeling of perfusion.

Myocardial perfusion is strongly modulated by cardiac contraction, with flow primarily occurring during diastole, a phenomenon referred to as systolic inhibition.[4] Furthermore, perfusion is regionally organized, reflecting distinct coronary supply territories,[12,18] which is critical for local disease assessment. While incorporating these factors enhances realism, it has often led to computationally intensive models that rely on excessive assumptions and parameters not readily measurable in routine clinical settings.[19] Consequently, a practical need exists for tractable, clinically-oriented workflows that can integrate multiscale physiological modeling with standard and readily available clinical data.

In this study, we propose an integrated computational workflow to combine the multiple-network poroelastic theory (MPET) and the clinical data for myocardial perfusion modeling. MPET was previously applied and clinically validated in brain perfusion studies.[20–24] The central novelty of this work lies in the integration of patient-specific LV morphology and image-derived coronary perfusion flow as inputs to a multiple-network poroelastic model to estimate diastolic MBF distribution. This work provides a computational model built from routine clinical inputs to connect patient-specific anatomy with functional perfusion metrics.

II. METHODS

A. Clinical data collection and processing

Two subjects with no known myocardial perfusion-related diseases gave informed consent before participation: a 25-year-old female (S1) and a 64-year-old male (S2). High-resolution myocardial structural sequences and first-pass perfusion sequences were acquired, and the detailed parameters are provided in the supplementary material (Sec. I).

For the structural images, a semi-automated reconstruction was performed using threshold-based and manual segmentation. The reconstructed geometry encompassed the entire left ventricular (LV) myocardium and was verified by a senior clinician with over a decade of experience in cardiac image interpretation and anatomical delineation. The pericardium and papillary muscles were excluded, consistent with similar clinical analyses.[13] The geometric models were discretized into surface triangular and volumetric tetrahedral elements using ANSYS ICEM CFD (ANSYS Inc.). The mesh resolution satisfied the convergence criteria provided in the supplementary material (Sec. II). The final LV myocardial mesh contained approximately 200 000 elements and was further extracted with endocardial (inner surface) and epicardial (outer surface) grids as boundaries, as shown in Fig. 1(b). Subsequently, the model was divided into 17 segments based on the American Heart Association (AHA) standard for boundary condition setup. For data analysis, the apical segment (17) was excluded following common clinical practice,[25] and analysis focused on the remaining segments ($\sigma = 1,\ldots,16$).

For the first-pass perfusion sequences, the post-processing involved both semi-quantitative and quantitative analyses performed using CVI42 (circle cardiovascular inc.). In the semi-quantitative analysis of normal-dose sequences, myocardial signal intensity (SI) was extracted from both the endocardial and epicardial borders of each segment to quantify transmural perfusion gradients (TPG), as defined in the following equations:

$$\left\langle \mathrm{SI}_{\Omega,\sigma}(t)\right\rangle = \frac{1}{3}\sum_{n=0}^{2}\mathrm{SI}_{\Omega,\sigma}(t)(n), \quad \Omega \in \{\mathrm{endo},\ \mathrm{epi}\}, \tag{1}$$

$$\mathrm{TPG}_{\sigma} = \frac{\left\langle \mathrm{SI}_{\mathrm{endo},\sigma}(t)\right\rangle}{\left\langle \mathrm{SI}_{\mathrm{epi},\sigma}(t)\right\rangle}. \tag{2}$$

The average signal intensity $\left\langle \mathrm{SI}_{\Omega,\sigma}(t)\right\rangle$ was computed for each myocardial segment σ ($\sigma = 1, \ldots, 16$) and region Ω (endocardial or epicardial), by averaging signals from sampling regions n at 0% ($n = 0$), 5% ($n = 1$), and 10% ($n = 2$) inwards from the respective boundary [Fig. 1(e)], over a steady enhancement period t (frames 30–50) following the first-pass peak. This sampling approach, common in clinical and quantitative analysis, was adopted to enhance signal robustness and mitigate artifacts from partial-volume effects and blood–pool contamination.[26] The TPG in a specific segment σ was then defined as the ratio of endocardial to epicardial average signal intensity.[27] This clinical TPG derived from image SI served as the benchmark. In contrast, the model derived TPG was calculated from a different quantity: the ratio of endocardial to epicardial MBF. For quantitative analysis, low-dose acquisitions were used to derive the arterial input function (AIF), which was then combined with myocardial SI data to compute MBF. Voxel-wise MBF maps were generated and extracted using a custom script for further analysis.

B. Multiple-network poroelastic theory for myocardial perfusion

The MPET framework is a computational tool for modeling the transport mechanisms of multiple fluid networks through a poroelastic medium, especially the interaction between different fluid networks and fluid–structure interaction at different scales, all at the same time in one integrated framework. This overcomes the limitation of analyzing fluid compartments separately, which is particularly important for perfused tissue. The MPET framework has been preliminarily applied in myocardial perfusion assessment,[28] demonstrating promising capability due to its flexibility and scalability.

The MPET myocardial model considers the myocardium as a deformable porous medium, with three coupled fluid networks: the

16 January 2026 16:04:00

© Author(s) 2026

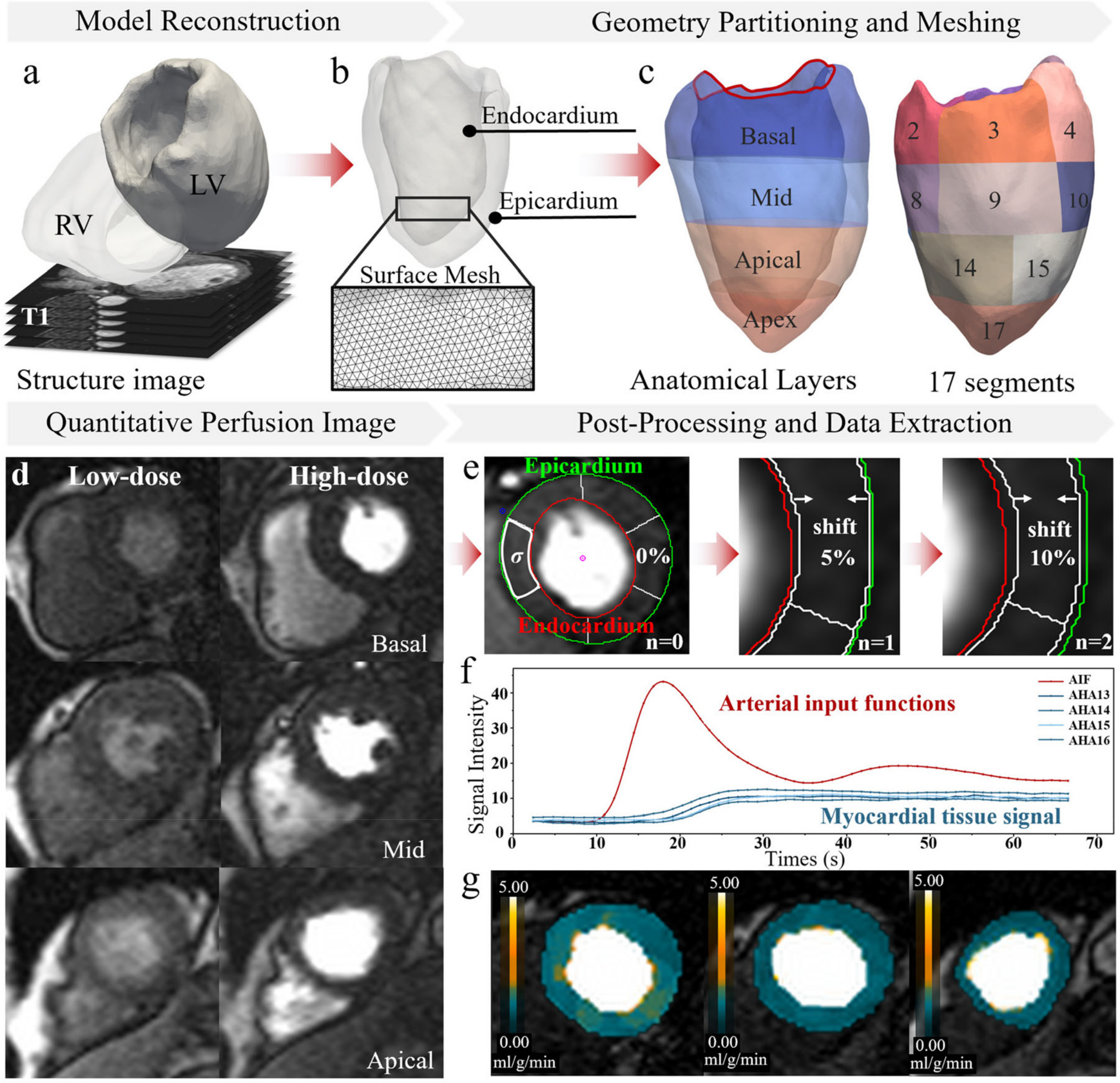

FIG. 1. Workflow of model reconstruction and quantitative perfusion analysis from clinical magnetic resonance (MR) imaging. Structural images were used to reconstruct the left ventricular (LV) and right ventricular (RV) models (a), define endocardial and epicardial surfaces and generate meshes (b), and segment the myocardium into 17 American Heart Association (AHA) segments (c). The red line denotes the basal epicardial region where displacement constraints were imposed. Perfusion images supported model validation (d)–(g): dual-bolus scans provided low- and high-dose slices (d); myocardial regions were segmented (with σ denoting a specific segment) and shifted inwards to extract signals across the myocardial wall (e) [see definitions in Eq. (1)]; signal intensities were extracted to compute transmural gradients (f); and to generate voxel-wise MBF maps (g).

arterial network (a), the arteriole/capillary network (c), and the venous network (v). Figure 2(c) illustrates the directional flows between networks, where networks are connected with each other.

C. Governing equations

The governing equations for the multiple-network poroelastic model have been described in detail in previous studies.[22,23] Here, we adapt them to the three-fluid-network model used in this paper. The governing equations of the 3-MPET myocardial model are described below.

$$G\nabla^2\mathbf{u} + (G+\lambda)\nabla\varepsilon = \alpha_a\nabla p_a + \alpha_c\nabla p_c + \alpha_v\nabla p_v, \tag{3}$$

$$S_a\frac{\partial p_a}{\partial t} + \alpha_a\frac{\partial\varepsilon}{\partial t} = \frac{k_a}{\mu_a}\nabla^2 p_a + s_{ca}, \tag{4}$$

$$S_c\frac{\partial p_c}{\partial t} + \alpha_c\frac{\partial\varepsilon}{\partial t} = \frac{k_c}{\mu_c}\nabla^2 p_c + (s_{ac} + s_{vc}), \tag{5}$$

$$S_v\frac{\partial p_v}{\partial t} + \alpha_v\frac{\partial\varepsilon}{\partial t} = \frac{k_v}{\mu_v}\nabla^2 p_v + s_{cv}. \tag{6}$$

The equilibrium equation, Eq. (3), describes the momentum balance of the porous medium, where G is the shear modulus; $\mathbf{u}$ is the

16 January 2026 16:04:00

© Author(s) 2026

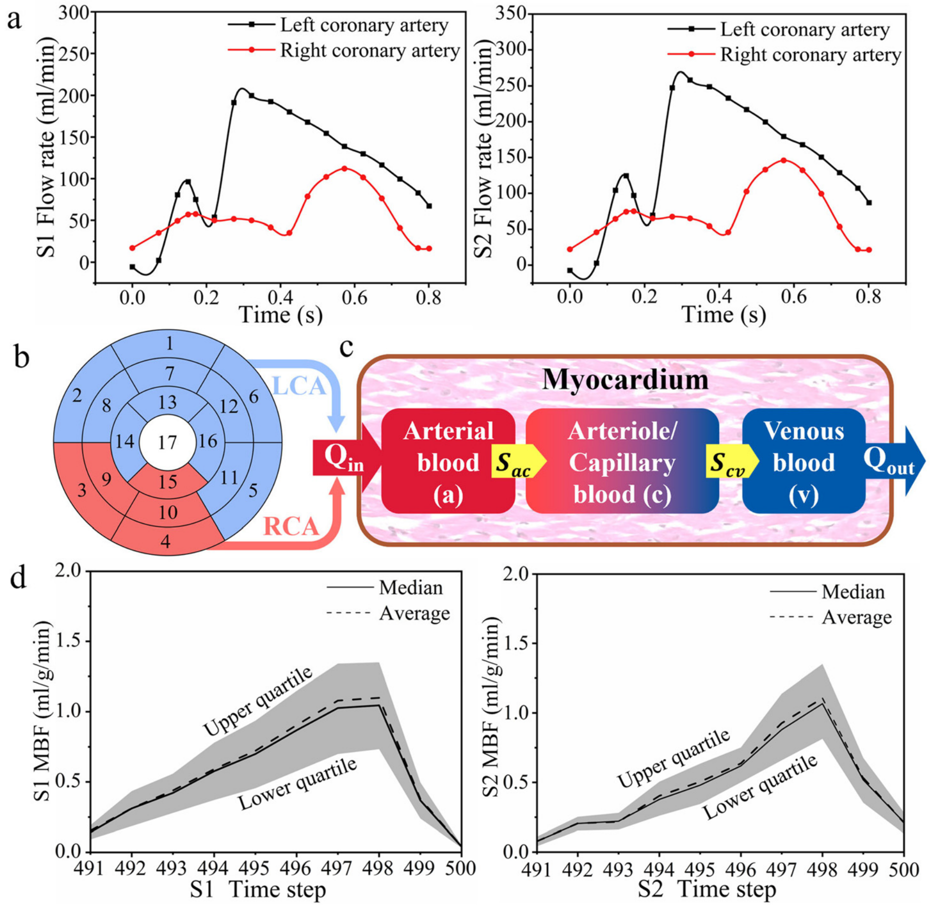

FIG. 2. Model input and output characteristics. (a) Inflow profiles for two subjects (S1 and S2); (b) perfusion territories supplied by the left coronary artery (LCA) and right coronary artery (RCA); (c) directional transport within the intramyocardial fluid network; and (d) myocardial blood flow (MBF) characteristics in the final cycle, with the peak values observed at time step 498.

tissue displacement; λ is the Lamé's constant; ε is the dilatational strain; $p_i\,(i = a, c,$ and $v)$ represent the pressure of each blood network. The Biot–Willis coefficient $\alpha_i\,(i = a, c,$ and $v)$ for each fluid network satisfy the relation with the total porosity $\varphi\,(\varphi \leq \alpha_a + \alpha_c + \alpha_v \leq 1)$.[29] Body forces (such as gravity) and inertia terms are neglected under the assumption of low acceleration frequencies.[30] The continuity equations, Eqs. (4)–(6), are used to describe mass conservation and fluid flow in the 3-MPET myocardial model. The specific storage $S_i\,(i = a, c,$ and $v)$ represents the measurement of the released fluid volume per unit pressure in the control volume under constant strain for each fluid compartment. The cross-porosity storage effect $(S_{ij}, i = a, c, v, j = a, c, v, i \neq j)$, which means the microscopic coupling effect between the volumetric deformation of different pore systems, is not considered in this study, due to the lack of accurate experimental data to quantify the coupling terms between different fluid networks in a physiological sense. The viscosity of each blood network is denoted by $\mu_i\,(i = a, c, v)$. The permeability $k_i\,(i = a, c,$ and $v)$ of each blood network is defined as the ability of fluid to permeate through a porous medium, and it is assumed to be isotropic in this study.[7]

In Eqs. (4)–(6), the source $(s_{ij} > 0)$ or sink $(s_{ij} < 0)$ term[30] is driven by a hydrostatic pressure gradient $s_{ij} = \omega_{ij}(p_i - p_j)$ and is scaled by the transfer coefficient ω_{ij}, which determines the blood flow from network i to network j. The directionality between blood compartments is derived from physiological considerations and required to follow the law of continuity.[7] Finally, Eqs. (7) and (8) describe the blood going from the arterial network into the arteriole/capillary network and then into the venous network.

$$s_{ac} = -s_{ca} = |s_{ac}| \geq 0, \tag{7}$$

$$s_{cv} = -s_{vc} = |s_{cv}| \geq 0. \tag{8}$$

$$\nabla p_a \mathbf{n} = Q_a \tag{9}$$

$$\nabla p_c \mathbf{n} = 0 \tag{10}$$

$$p_v = p_{CS} \tag{11}$$

$$\nabla p_a \mathbf{n} = 0 \tag{12}$$

$$\kappa_c \nabla p_c \mathbf{n} = -\beta Q_a \tag{13}$$

$$\nabla p_v \mathbf{n} = 0 \tag{14}$$

In this study, the computational domain is the LV myocardium, which has been established as the primary region of interest for perfusion analysis in clinical practice and in computational modeling studies.[31]

D. Boundary conditions and material properties

The myocardium accounts for most of the LV wall thickness and is primarily responsible for its mechanical behavior.[32] The epicardium

16 January 2026 16:04:00

© Author(s) 2026

TABLE I. Boundary conditions used in the 3-MPET modeling.

	Epicardium	Endocardium
Displacement	No displacement constraints	No displacement constraints
Arterial blood	Eq. (9)	Eq. (12)
Arteriole/Capillary blood	Eq. (10)	Eq. (13)
Venous blood	Eq. (11)	Eq. (14)

and endocardium are the outer and inner surfaces of the myocardium, respectively, and serve as boundaries of the computational domain. The pericardium was excluded from our perfusion analysis, as the lubricating serous fluid minimizes friction, and perfusion-induced deformations were considered too small to generate significant constraint forces. The 3-MPET framework enables flexible definition of solid and fluid phase boundary conditions based on physiological requirements. The heart-specific fluid and solid boundary conditions implemented in 3-MPET are detailed in Table I.

Table I specifies the displacements required for modeling, with no restriction to the possible movement of the endocardium and epicardium. However, to avoid free body movement and unphysiological results, we followed an approach similar to that of Lee *et al.*,[13] fixing nodes at the superior edge of the basal epicardium of the LV [Fig. 1(c)]. The arterial blood flow on the epicardial surface is simplified into a flux boundary condition [Neumann boundary condition, Fig. 2(a)] Q_a, supplied by the left coronary artery (LCA) and right coronary artery (RCA). The pulsatile waveform and coronary flow fractions – 2.67% of stroke volume (SV) for the LCA and 1.33% for the RCA – were derived from Doppler ultrasound data,[33] then scaled to each subject's SV (Table II), which was measured from clinical imaging. Based on the AHA segmentation model, the myocardium is divided into 17 segments and supplied by different coronary arteries.[34] The myocardial segmentation and corresponding coronary artery supply segments in this study are shown in Fig. 2(b).

For the arteriole/capillary compartment, the right-hand side of Eq. (13) represents the decrease in arteriole/capillary pressure resulting from blood flow to the venous network, where κ_c denotes the capillary-to-venous resistance. The coefficient β $(0 \leq \beta \leq 1)$ defines the proportion of capillary outflow that exits directly through the endocardial surface via the besian veins or the subendocardial venous plexus, which typically accounts for only a small fraction of total venous drainage.[35] The majority of blood returns through the epicardial veins into the coronary sinus and subsequently into the right atrium. Accordingly, the venous boundary condition at the epicardial surface was set to the coronary sinus pressure (p_{CS}), taken as 665 Pa (5 mm Hg) based on previous studies.[36] In this manner, the model's boundary conditions for both arterial supply and venous drainage are defined by key anatomical locations and physiological flow directions.

Table II lists the poroelastic parameters and corresponding values applied in the 3-MPET myocardial modeling. The shear modulus G and the Lamé's constant λ were deduced from Young's modulus (E) and Poisson's ratio (ν). The MPET model includes predefined initial values from our previous work.[30] When adapted to myocardial tissue, a sensitivity analysis was performed to evaluate the influence of these parameters. The results, provided in the supplementary material (Sec. III), showed that not all parameters had a significant impact on the outputs of interest. Specifically, the parameters α_i, ω_{ac}, ω_{cv}, and κ_c showed low sensitivity, suggesting a limited role for fluid perfusion in the myocardium, consistent with the expectations in a physiological sense. The insensitive behavior of these parameters enhanced model flexibility and scalability, allowing cross-scenario applicability without requiring extensive experimental datasets. In contrast, permeability (k) and Young's modulus (E) were identified as key parameters, directly associated with mechanical properties and measurable through clinical techniques, such as magnetic resonance elastography (MRE). In this initial study, both were assumed isotropic and homogeneous to validate the subject-specific workflow and assess the physiological plausibility of the results. Based on the modeling assumptions and the diastolic phase, Young's modulus was set to be 20 kPa as it yields physiologically realistic passive deformations in the millimeter range (see supplementary material, Fig. S3). Sensitivity analysis further showed that variations in Young's modulus introduced only mild changes in the flow magnitude, while the spatial perfusion pattern remained essentially unchanged. This behavior is consistent with the expected weak solid–fluid coupling under late-diastolic small-strain conditions. Permeability ($k = 1.0 \times 10^{-10}$ m^2) was determined through a sensitivity analysis (see supplementary material, Fig. S4), achieving a balance between physiological considerations and numerical stability. Poisson's ratio was assigned a value of 0.35 (Ref. 37) to accommodate ventricular dilatation. To ensure generalizability and facilitate practical applications, these critical parameters are encapsulated as independent modules for streamlined calibration.

TABLE II. Poroelastic parameters used in the 3-MPET myocardial modeling.

Parameters	Values	Units		Parameters	Values	Units	
α_a	0.25		22	S_a	2.9×10^{-4}	$\mathrm{m^2N^{-1}}$	22
α_c	0.25		22	S_c	2.9×10^{-4}	$\mathrm{m^2N^{-1}}$	22
α_v	0.01		22	S_v	1.5×10^{-5}	$\mathrm{m^2N^{-1}}$	22
ν	0.35			$k_{a,c,v}$	1.0×10^{-10}	$\mathrm{m^2}$	22
E	20	kPa		ω_{ac}	1.5×10^{-7}	$\mathrm{m^2N^{-1}s^{-1}}$	30
β	0.01			ω_{cv}	1.5×10^{-7}	$\mathrm{m^2N^{-1}s^{-1}}$	30
SV1	57.7	ml		p_{CS}	665	Pa	36
SV2	75.0	ml		κ_c	6.0×10^{-4}	$\mathrm{m^6N^{-1}s^{-1}}$	21

16 January 2026 16:04:00

© Author(s) 2026

E. Numerical implementation

MPET simulations were performed for two subjects. The governing equations are discretized by the finite element method and implemented in an in-house Fortran code. The displacement field $\mathbf{u}$ and the pressures p_i $(i = a, c,$ and $v)$ of the three fluid networks are calculated in the space of continuous piecewise linear polynomials. The discrete equilibrium equation is derived from the principle of minimum potential energy. The continuity equations of the fluid networks are discretized using the weighted residuals method and the continuous Galerkin formulation. The temporal discretization of the governing equations is implemented using the implicit backward Euler scheme. In this paper, one cardiac cycle was divided into 10 time-steps and the same cycle was repeated 50 times to reach a steady state. More specifically, for each time step, the pressure and displacement solutions of the discretized equations are solved in a tightly coupled manner until subsequent cycles only generate negligible differences. Convergence is achieved when residuals fall below 10^{-3}. More detailed description of this in-house solver was specified in our previous work.[22]

The MPET model is formulated using displacements and fluid pressures as primitive variables, with all other quantities obtained through post-processing. In this study, the Darcy's law is used to calculate the velocity for the three fluid networks at the end of each time step.

$$\mathbf{v}_i = -\frac{k}{\mu}\nabla p, \tag{15}$$

where $\mathbf{v}_i$ is the Darcy velocity for each fluid network $(i = a, c,$ and $v)$ and represents the volume of fluid passing a unit area per unit time. Considering the inhibition during systole, myocardial perfusion predominantly occurs during diastole.[4] Therefore, the analyses in this paper focused on the diastolic peak of the final cardiac cycle [time step 498, Fig. 2(d)] to represent steady-state perfusion.

III. RESULTS

The MPET framework can output multiple variables for fluid and solid phases. This study focuses on clinically relevant outputs. More specifically, the Darcy velocity of the arteriole/capillary network, also known as the filtration velocity, can be used to represent the MBF. MBF is typically measured in ml/g/min, whereas filtration velocity is measured in m/s. To enable direct comparison, the filtration velocity can be converted into MBF by being divided by the density of myocardial tissue (1.05 g/cm^3)[38] and a characteristic length scale of the myocardial tissue thickness. The following results correspond to the diastolic phase and reflect the primary myocardial perfusion under zero left ventricular pressure, as assumed in the simplified model.

MBF for the two models were 0.95 ± 0.28 ml/g/min for S1 and 1.01 ± 0.29 ml/g/min for S2, respectively, both within the normal physiologic range. Fairbairn *et al.*[39] reported resting MBF values of 0.97 ± 0.40 ml/g/min in 19 healthy nonsmokers, and Hughes *et al.*[40] reported 0.87 ml/g/min (95% CI: 0.80–1.00) in 32 healthy volunteers. Relatively lower MBF values were observed at the basal and apical regions [Fig. 3(a)], which may reflect the influence of imposed displacement constraints [red line in Fig. 1(c)]. The 17-segment model of AHA was used to create a bullseye map in Fig. 3(b), which shows the mean MBF for each individual segment. Additionally, Fig. 3(c) shows the bullseye map of diastole wall thickness measured from structural imaging. Due to the limitations in scan time and spatial resolution, clinical CMR perfusion imaging typically acquires only three key short-axis slices. S1 obtained only standard-dose perfusion imaging, which is prone to signal saturation[41] and therefore unsuitable for accurate MBF quantification and not presented in Fig. 3(c).

For S2, voxel-wise MBF was calculated from perfusion images [Fig. 1(g)], and the color bar was adjusted to match the model output for more direct comparison. Partial agreement in regional perfusion distribution is observed, especially regarding the spatial alignment of perfusion zones (red arrows). However, since the subject did not exhibit apparent perfusion defects and the spatial resolution of the clinical images was limited, the overall contrast between the two modalities is relatively subtle. By comparison, the simulated results show a larger difference between high and low perfusion regions, indicating greater sensitivity of the model to local perfusion heterogeneity. Clinical quantitative MBF values may vary with imaging resolution and post-processing steps; hence, the comparison here mainly focuses on the spatial distribution pattern.[42]

To quantify the relationship between local myocardial wall thickness and MBF, the left ventricular myocardium was sampled at high spatial density by dividing the model into angular sectors circumferentially and longitudinal segments from apex to base. At each sampling location, wall thickness was defined as the shortest Euclidean distance from a point on the endocardial surface to the nearest corresponding point on the epicardial surface. The MBF at the same location was calculated as the transmural average across all nodes between the endocardium and epicardium, yielding approximately 800 paired measurements.

Correlation analysis [Fig. 5(a)] revealed a statistically significant but weak negative association between myocardial wall thickness and MBF in both subjects (S1: $r = -0.1786$; S2: $r = -0.1363$; both $P < 0.0001$). The robustness of this trend was confirmed through sensitivity analyses with varying sampling densities and outlier exclusion criteria (0%–5%). Analysis using 95% prediction bands showed that no regional values fell below the lower bound, indicating a defined lower limit of perfusion and the absence of abnormally low-perfusion regions. All mid-ventricular data points were contained within the prediction bands, demonstrating consistent model performance in this central functional region of the heart.

Myocardial perfusion typically exhibits a transmural gradient, with an endocardial MBF slightly higher than that of the epicardium. This physiological perfusion heterogeneity was also observed in our simulation results [Figs. 3(a), 4(a), and 4(b)]. To further examine whether the model captured this physiological feature, the TPG was calculated as an auxiliary validation metric. In the simulation, TPG was defined as the ratio of endocardial to epicardial MBF, whereas for clinical perfusion images, the TPG was derived based on SI signal intensity as described in Sec. II A. Due to these methodological differences, the relative distribution and directional trends of TPG are more meaningful for interpretation than direct numerical comparison. As shown in Fig. 5, all segments exhibited $\mathrm{TPG} > 1$, indicating that the model reproduced the expected transmural perfusion gradient. While several segments showed similar regional patterns between simulations and clinical images [Fig. 5(b)], the overall correspondence was modest, likely reflecting both the differences in perfusion-signal extraction and the simplified physiological representation in the current model.

During diastole, the myocardium remains mechanically passive, with the arterial inflow and the negligible venous outflow. Since S1 was used for parameter testing and showed numerically similar results to

16 January 2026 16:04:00

© Author(s) 2026

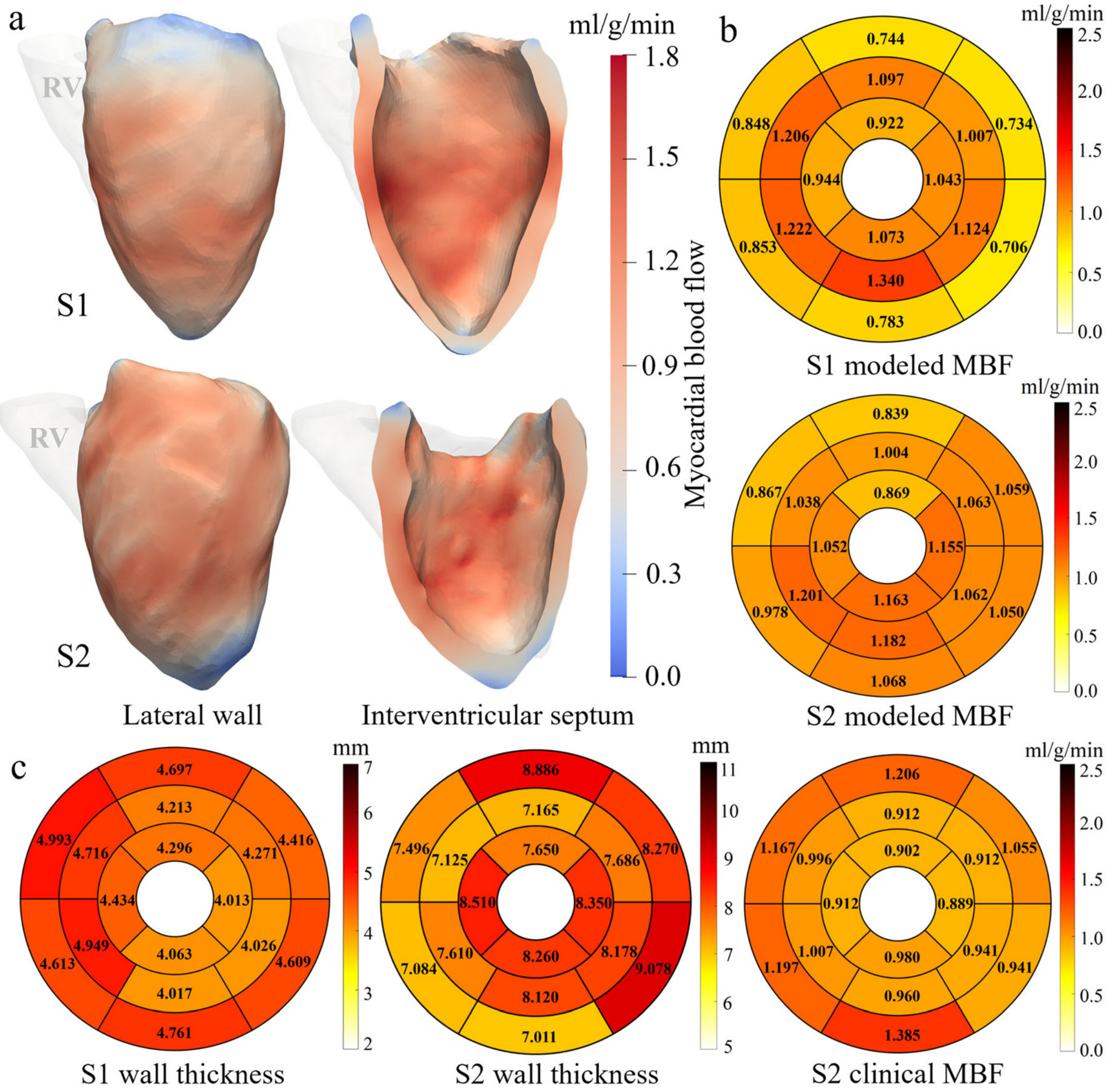

FIG. 3. Simulated and measured myocardial blood flow (MBF) at rest during diastole and myocardial wall thickness. (a) Simulated MBF for S1 and S2; (b) bullseye maps showing average simulated MBF across 16 segments (excluding the apex); and (c) bullseye maps of segmental average wall thickness from structural imaging (S1 and S2), and MBF from perfusion imaging (S2).

S2, only S2 is presented here. As shown in Figs. 6(a) and 6(c), arterial pressure (∼58 mm Hg) is slightly higher at the apex compared to the base. In contrast, arteriolar/capillary pressures (∼47 mm Hg) exhibit an inverse spatial pattern, i.e., higher at the base. Venous pressure was approximately 675 Pa (∼5 mm Hg), showing a gradual radial gradient from endocardium to epicardium, consistent with the direction of venous drainage. The computed coronary perfusion pressure, defined as the gradient between coronary inflow and outflow, is 110 mm Hg, well within the physiological range of 46–124 mm Hg.[43] The pressure outputs in the simulation results can be justified by previously published data, which report typical arteriole/capillary pressures of 20–30 mm Hg, and venous pressures around 10 mm Hg.[7] Figure 6(d) shows myocardial deformation induced by perfusion rather than contraction in the MPET myocardial model, with maximal deformation of 5.5 mm at the apex and negligible deformation at the base. For tissue deformation, although direct validation remains limited, the observed distribution and magnitude of displacement are anatomically reasonable and consistent with previous findings from *ex vivo* heart models.[44,45]

IV. DISCUSSION

This study applies the MPET framework to simulate myocardial perfusion, establishing a workflow that is capable of integrating clinical imaging data and deriving clinically interpretable

16 January 2026 16:04:00

© Author(s) 2026

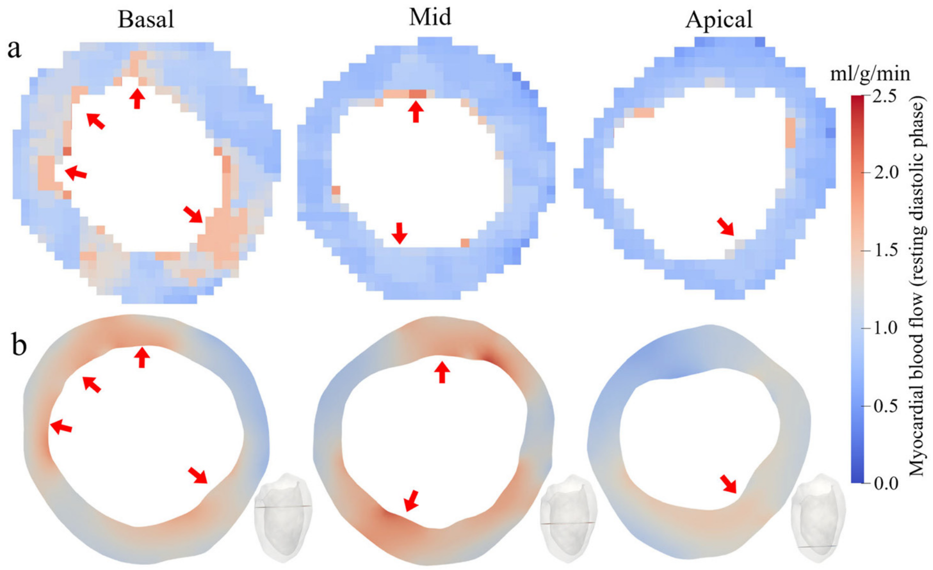

FIG. 4. Comparison between perfusion imaging and simulation at rest during diastole. (a) Myocardial blood flow extracted from perfusion imaging (S2) and (b) modeled myocardial blood flow at the corresponding slices. Red arrows highlight partial agreement in regional perfusion distribution.

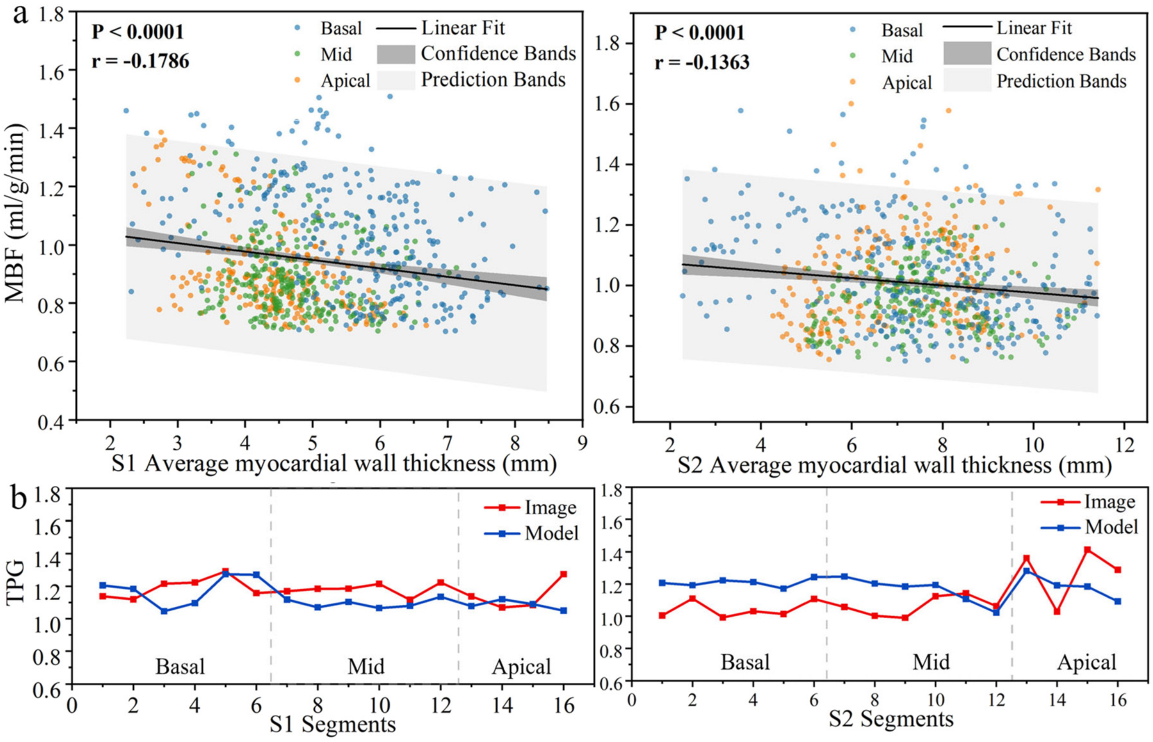

FIG. 5. (a) Correlation between local myocardial wall thickness and simulated myocardial blood flow (MBF); (b) comparison of the segmental transmural perfusion gradient (TPG) between the simulation model and clinical imaging data.

perfusion indices. The model assumes the myocardium as a deformable tissue containing three interacting fluid networks (arterial, arteriole/capillary, and venous). The framework incorporates physiologically informed flow boundary conditions that reflect the distinct inflow and outflow characteristics of coronary circulation, ensuring a realistic representation of myocardial blood distribution and directional exchange across the tissue. This model provides a workflow that translates anatomical data into functional

16 January 2026 16:04:00

© Author(s) 2026

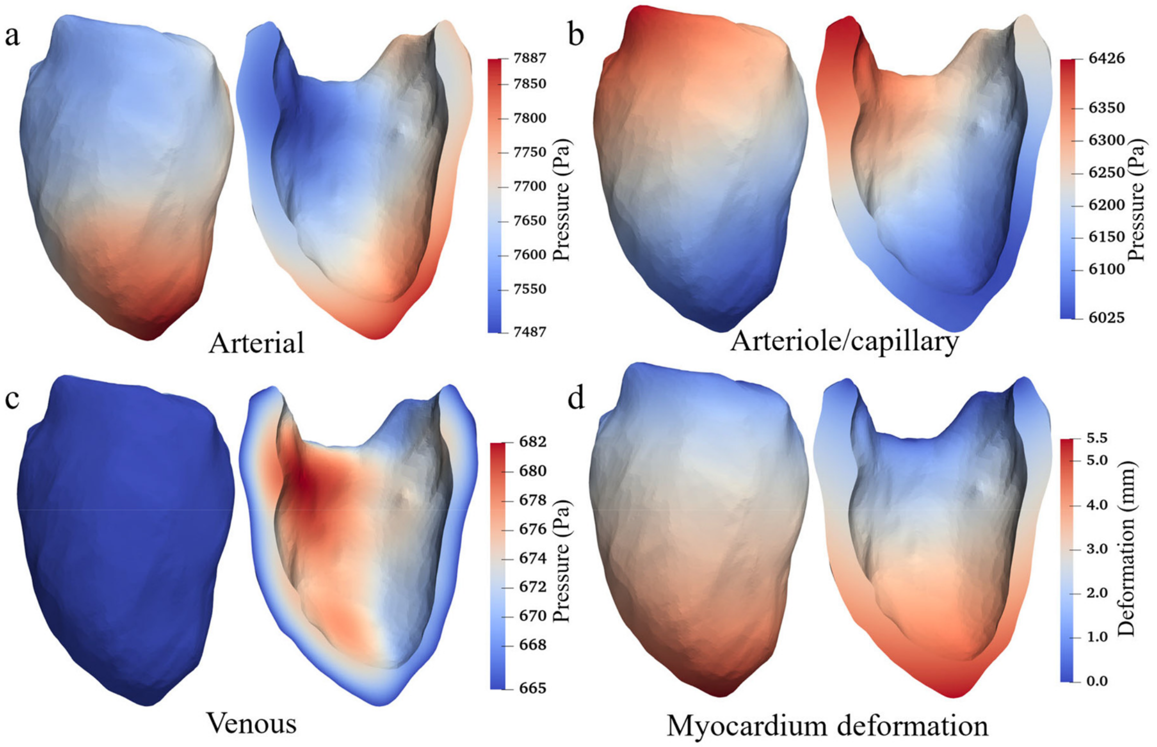

FIG. 6. Simulated pressure distribution and myocardial deformation of S2. (a)–(c) Simulated pressures in the arterial, arteriole/capillary, and venous networks; (d) Simulated myocardial deformation.

perfusion measures, which were preliminarily validated against clinical imaging data.

The proposed model generates clinically relevant myocardial perfusion metrics using subject-specific inputs, including myocardial geometry and stroke volume, which are readily available from standard clinical imaging. This workflow translates anatomical structure into functional output without the need for contrast agents, while delivering high spatial resolution and comprehensive three-dimensional perfusion mapping. High-fidelity frameworks, such as those by Lee *et al.*[13] and Cookson *et al.*,[16] incorporate finite–strain mechanics and active contraction, enabling comprehensive analysis of whole-cycle coronary hemodynamics and wave propagation. In parallel, multiscale studies (e.g., Papamanolis *et al.*,[15] Di Gregorio *et al.*[4]) emphasize patient-specific vascular anatomy, which typically employ porous–media formulations (ranging from single- to multi-compartment models) where the myocardium is simplified as a rigid matrix to prioritize vascular topology over tissue mechanics. The present study focuses specifically on the diastolic myocardial perfusion, where the interplay between tissue deformation and multi-compartment fluid exchange is retained. This rationale emphasizes the mechanical link between passive myocardial properties and perfusion as disease processes, such as fibrosis, primarily manifest through alterations in tissue stiffness, which cannot be directly reflected in rigid porous media formulations. Although not fully investigated in diseased states, this workflow provides a potential computational tool for studying such pathological conditions. This capability allows for a more comprehensive characterization of the spatial heterogeneity of perfusion than conventional slice-based imaging.[46] In addition to standard indices, the model yields compartmental pressure and velocity distributions, which are rarely accessible in clinical practice yet could provide supplementary diagnostic insights. With further optimization and validation, these computationally derived indices may provide additional insights that could support clinical interpretation in future applications.

Our quantitative analysis establishes a consistent and statistically significant negative correlation between local myocardial wall thickness and MBF. Within the MPET framework, this is mechanistically plausible, as thicker myocardial segments increase local hydraulic resistance. The relative weakness of this correlation is also physiologically insightful, since regional perfusion is multifactorial and not solely determined by morphology.[47,48] This specific characteristic makes the model clinically meaningful for assessing conditions involving morphological remodeling, such as hypertrophic cardiomyopathy (HCM). It provides a quantitative pathway to distinguish perfusion reductions attributable to the mechanical effects of hypertrophy from those indicating a superimposed, and potentially more severe, microvascular dysfunction.[40,48] Furthermore, the framework enables direct quantification of TPG with full-heart, high-resolution coverage. TPG holds recognized clinical value as an early marker of coronary artery disease and is relevant to the heightened vulnerability of the subendocardium, which is more prone to perfusion deficits under structural remodeling or functional impairment.[49] The ability to facilitate earlier detection of pathological perfusion changes and enhance risk stratification is a key

16 January 2026 16:04:00

advantage of the proposed framework, aligning closely with pressing clinical needs.[40]

While this study demonstrates the potential of the MPET framework, several limitations must be acknowledged. First, due to the need for contrast agent administration in clinical CMR perfusion, this study was limited to a small cohort of two healthy subjects, thereby restricting the generalizability of our findings. Some discrepancies were observed between the model results and the clinical imaging data, which may be partly attributable to the simplified physiological assumptions used in the current model, as well as variation in quantitative MBF estimation from perfusion CMR. To further capture pathological results, these assumptions would need refinement, and the outputs would require more quantitative and rigorous validation. In this initial implementation, only a subset of the model's output variables was directly validated. Future studies involving larger and more diverse cohorts, including patients with pathological conditions, are essential to fully assess model robustness and clinical utility.

It should be emphasized that the primary goal of the present study is to validate a subject-specific workflow using a simplified MPET-based poroelastic model, rather than to provide a fully physiological, full-cycle cardiac mechanics simulation. From a modeling perspective, while the integrated MPET framework is well-suited for capturing cross-scale fluid transport within the myocardium, the current implementation focuses only on the intramyocardial domain. To further enhance physiological realism, future work should account for the influence of the upstream epicardial network. Previous studies have shown that coupling coronary simulations with microvascular compartments yields more patient–specific inlet boundary conditions,[14,15] which can substantially affect downstream microvascular perfusion and therefore represent an important direction for improvement.

At present, the model analysis is limited to the diastolic phase, as approximately 85% of left ventricular perfusion occurs during this period. Nevertheless, such a simplification inevitably overlooks the dynamic effects of systolic–diastolic coupling, including variations in left ventricular pressure (LVP), intramyocardial pressure (IMP), and the time-dependent changes in myocardial material properties. During the cardiac cycle, the myocardium undergoes a rapid transition from the systolic state, characterized by high LVP ($\sim$120 mm Hg), elevated IMP, and increased active stiffness, to a relaxed and compliant diastolic state with low LVP ($\sim$10 mm Hg).[50] This rapid unloading facilitates microvascular reopening and induces a suction effect within the microcirculation, which serves as a key driving force for early diastolic perfusion.[51] Therefore, the current implementation represents a simplified diastolic condition that decouples the perfusion process from these complex interactions by directly prescribing the measured, diastolic-dominant coronary flow waveform as the inflow boundary condition. This simplification was adopted because the present stage of this work is primarily aimed at establishing a subject-specific workflow that translates clinical imaging data into baseline perfusion parameters. Extending the framework to incorporate these coupled effects, such as LVP dynamics and finite-strain mechanics, represents a critical next step. This advancement will involve addressing the common challenge of balancing physiological fidelity, computational complexity, and clinical applicability,[52] which remains a key consideration in our future developments.

Finally, the current implementation assumes isotropic material properties, particularly for permeability. Physiologically, myocardial fibers form a helical arrangement that varies transmurally. The microvascular network trends to align with this fiber orientation, implying that microvascular flow is anisotropic,[53] with potentially enhanced flow along fiber directions and impeded flow perpendicular to them. Consequently, this simplification likely results in discrepancies between the simulated MBF distribution and the true anisotropic flow patterns, particularly at small scales. While the model reproduces the physiological trend of higher endocardial perfusion, incorporating anisotropy could further refine this distribution. Another key simplification is the adoption of a linear elastic material model, even though cardiac tissue is inherently nonlinear.[11] This assumption is reasonable for the passive diastolic phase, where perfusion–induced deformations are expected to be small. Crucially, retaining the poroelastic coupling remains essential, as it links tissue properties with microvascular flow. These simplifications only reflect a limitation of the current implementation rather than inherent constraints of the framework itself. A major advantage of the MPET framework is its proven adaptability for multimodal data incorporation. Prior applications in cerebral perfusion successfully integrated patient-specific fiber orientations, heterogeneous and anisotropic permeability, and pathology-specific perfusion territories.[20,21,24] Building on this capability, future work could focus on implementing more subject-specific features into the myocardial model, such as fiber orientations from MR diffusion tensor imaging or tissue properties from MRE and T1 mapping, to improve physiological realism and disease-state prediction.

V. CONCLUSIONS

In conclusion, this study introduces a computational workflow for developing subject-specific myocardial perfusion models by integrating routine CMR imaging data with the multiple-network poroelastic theory. The integrated model captured key physiological characteristics of myocardial tissue and fluid networks, providing detailed quantification of flow, transport phenomena, transmural gradients, and tissue deformation. The core output MBF was preliminarily validated against CMR perfusion imaging data. This work represents an initial step toward a virtual evaluation platform, with the potential to reduce reliance on contrast agents or pharmacological stress testing. The framework allows for simulating diverse scenarios, such as stress test via adjusted boundary conditions, or the perfusion impact of morphological remodeling. This ability to computationally explore the heart's structure-function relationship suggests a promising pathway toward improved early disease detection and risk stratification.

SUPPLEMENTARY MATERIAL

See the supplementary material for cardiac MRI protocols for structural and perfusion imaging, mesh independence tests, parameter sensitivity tests, and references.

ACKNOWLEDGMENTS

This research was supported by the National Natural Science Foundation of China (Grant Nos. TT2425020 and U23A20484).

AUTHOR DECLARATIONS

Conflict of Interest

The authors have no conflicts to disclose.

16 January 2026 16:04:00

© Author(s) 2026

Ethics Approval

This study was approved by the Ethics Committee of Beijing Institute of Technology, Beijing, China (Approval No. BIT-EC-H-2024152). Clinical data were obtained from Fuwai Hospital, Chinese Academy of Medical Sciences, Beijing, China, through an established collaborative research framework. All human participants gave written informed consent before participating in the study.

Author Contributions

Xingyu Su: Formal analysis (equal); Writing – original draft (equal). **Zeyan Li:** Formal analysis (supporting); Writing – review & editing (equal). **Xin Yuan:** Data curation (lead). **Yuting Yang:** Data curation (supporting); Investigation (supporting). **Liwei Guo:** Conceptualization (equal); Writing – review & editing (equal). **Duanduan Chen:** Conceptualization (equal); Funding acquisition (lead); Supervision (equal).

DATA AVAILABILITY

The data that support the findings of this study are available from the corresponding authors upon reasonable request.

REFERENCES

[1] S. Godo, A. Suda, J. Takahashi, S. Yasuda, and H. Shimokawa, "Coronary microvascular dysfunction," Arterioscler., Thromb., Vasc. Biol. **41**, 1625 (2021).
[2] M. G. Del Buono, R. A. Montone, M. Camilli, S. Carbone, J. Narula, C. J. Lavie, G. Niccoli, and F. Crea, "Coronary microvascular dysfunction across the spectrum of cardiovascular diseases: JACC state-of-the-art review," J. Am. Coll. Cardiol. **78**, 1352 (2021).
[3] S. L. Waters, J. Alastruey, D. A. Beard, P. H. Bovendeerd, P. F. Davies, G. Jayaraman, O. E. Jensen, J. Lee, K. H. Parker, A. S. Popel, T. W. Secomb, M. Siebes, S. J. Sherwin, R. J. Shipley, N. P. Smith, and F. N. van de Vosse, "Theoretical models for coronary vascular biomechanics: Progress & challenges," Prog. Biophys. Mol. Biol. **104**, 49 (2011).
[4] S. Di Gregorio, M. Fedele, G. Pontone, A. F. Corno, P. Zunino, C. Vergara, and A. Quarteroni, "A computational model applied to myocardial perfusion in the human heart: From large coronaries to microvasculature," J. Comput. Phys. **424**, 109836 (2021).
[5] K. Terzaghi, *Theoretical Soil Mechanics* (John Wiley & Sons, New York, 1943).
[6] M. A. Biot, "Theory of propagation of elastic waves in a fluid-saturated porous solid. II. Higher frequency range," J. Acoust. Soc. Am. **28**, 179 (1956).
[7] D. Chapelle, J.-F. Gerbeau, J. Sainte-Marie, and I. Vignon-Clementel, "A poroelastic model valid in large strains with applications to perfusion in cardiac modeling," Comput. Mech. **46**, 91 (2010).
[8] J. M. Huyghe, T. Arts, D. H. van Campen, and R. S. Reneman, "Porous medium finite element model of the beating left ventricle," Am. J. Physiol. Heart Circ. Physiol. **262**, H1256 (1992).
[9] K. May-Newman and A. D. McCulloch, "Homogenization modeling for the mechanics of perfused myocardium," Prog. Biophys. Mol. Biol. **69**, 463 (1998).
[10] E. Y. Ng, D. N. Ghista, and R. C. Jegathese, "Perfusion studies of steady flow in poroelastic myocardium tissue," Comput. Methods Biomech. Biomed. Eng. **8**, 349 (2005).
[11] A. T. Vuong, L. Yoshihara, and W. A. Wall, "A general approach for modeling interacting flow through porous media under finite deformations," Comput. Methods Appl. Mech. Eng. **283**, 1240 (2015).
[12] N. A. Barnafi Wittwer, S. D. Gregorio, L. Dede, P. Zunino, C. Vergara, and A. Quarteroni, "A multiscale poromechanics model integrating myocardial perfusion and the epicardial coronary vessels," SIAM J. Appl. Math. **82**, 1167 (2022).
[13] J. Lee, D. Nordsletten, A. Cookson, S. Rivolo, and N. Smith, "In silico coronary wave intensity analysis: Application of an integrated one-dimensional and poromechanical model of cardiac perfusion," Biomech. Model. Mechanobiol. **15**, 1535 (2016).
[14] G. Montino Pelagi, A. Baggiano, F. Regazzoni, L. Fusini, M. Ali, G. Pontone, G. Valbusa, and C. Vergara, "Personalized pressure conditions and calibration for a predictive computational model of coronary and myocardial blood flow," Ann. Biomed. Eng. **52**, 1297 (2024).
[15] L. Papamanolis, H. J. Kim, C. Jaquet, M. Sinclair, M. Schaap, I. Danad, P. van Diemen, P. Knaapen, L. Najman, H. Talbot, C. A. Taylor, and I. Vignon-Clementel, "Myocardial perfusion simulation for coronary artery disease: A coupled patient-specific multiscale model," Ann. Biomed. Eng. **49**, 1432 (2021).
[16] A. Cookson, J. Lee, C. Michler, R. Chabiniok, E. Hyde, D. Nordsletten, M. Sinclair, M. Siebes, and N. Smith, "A novel porous mechanical framework for modelling the interaction between coronary perfusion and myocardial mechanics," J. Biomech. **45**, 850 (2012).
[17] J. Lee and N. P. Smith, "The multi-scale modelling of coronary blood flow," Ann. Biomed. Eng. **40**, 2399 (2012).
[18] S. Heath Richardson, J. Mackenzie, N. Thekkethil, L. Feng, J. Lee, C. Berry, N. A. Hill, X. Luo, and H. Gao, "Cardiac perfusion coupled with a structured coronary network tree," Comput. Methods Appl. Mech. Eng. **428**, 117083 (2024).
[19] G. Montino Pelagi, F. Regazzoni, J. M. Huyghe, A. Baggiano, M. Ali, S. Bertoluzza, G. Valbusa, G. Pontone, and C. Vergara, "Modeling cardiac microcirculation for the simulation of coronary flow and 3D myocardial perfusion," Biomech. Model. Mechanobiol. **23**, 1863 (2024).
[20] L. Guo, J. C. Vardakis, T. Lassila, M. Mitolo, N. Ravikumar, D. Chou, M. Lange, A. Sarrami-Foroushani, B. J. Tully, Z. A. Taylor, S. Varma, A. Venneri, A. F. Frangi, and Y. Ventikos, "Subject-specific multi-poroelastic model for exploring the risk factors associated with the early stages of Alzheimer's disease," Interface Focus **8**, 20170019 (2018).
[21] L. Guo, Z. Li, J. Lyu, Y. Mei, J. C. Vardakis, D. Chen, C. Han, X. Lou, and Y. Ventikos, "On the validation of a multiple-network poroelastic model using arterial spin labeling MRI data," Front. Comput. Neurosci. **13**, 60 (2019).
[22] L. Guo, J. C. Vardakis, D. Chou, and Y. Ventikos, "A multiple-network poroelastic model for biological systems and application to subject-specific modelling of cerebral fluid transport," Int. J. Eng. Sci. **147**, 103204 (2020).
[23] J. C. Vardakis, G. Valbusa, L. Guo, T. W. Peach, T. Lassila, M. Mitolo, D. Chou, Z. A. Taylor, S. Varma, A. Venneri, and A. F. Frangi, "Fluid–structure interaction for highly complex, statistically defined, biological media: Homogenisation and a 3D multi-compartmental poroelastic model for brain biomechanics," J. Fluids Struct. **91**, 102641 (2019).
[24] Z. Li, D. Chen, Z. Li, H. Fan, L. Guo, B. Sui, and Y. Ventikos, "A computational study of fluid transport characteristics in the brain parenchyma of dementia subtypes," J. Biomech. **159**, 111803 (2023).
[25] J. Schwitter, C. M. Wacker, A. C. van Rossum, M. Lombardi, N. Al-Saadi, H. Ahlstrom, T. Dill, H. B. W. Larsson, S. D. Flamm, M. Marquardt, and L. Johansson, "MR-IMPACT: Comparison of perfusion-cardiac magnetic resonance with single-photon emission computed tomography for the detection of coronary artery disease in a multicentre, multivendor, randomized trial," Eur. Heart J. **29**, 480 (2008).
[26] Y. J. Hong, K. Han, H. J. Lee, J. Hur, Y. J. Kim, M. J. Kim, and B. W. Choi, "Assessment of feasibility and interscan variability of short-time cardiac MRI for cardiotoxicity evaluation in breast cancer," Radiol. Cardiothorac. Imaging **6**, e220229 (2024).
[27] G. Hautvast, A. Chiribiri, T. Lockie, M. Breeuwer, E. Nagel, and S. Plein, "Quantitative analysis of transmural gradients in myocardial perfusion magnetic resonance images," Magn. Reson. Med. **66**, 1477 (2011).
[28] X. Su, Z. Li, X. Yuan, H. Wang, L. Guo, and D. Chen, *Multiple-Network Poroelastic Model for Subject-Specific Myocardial Perfusion Simulation* (SPIE, 2024).
[29] J. G. Berryman, "Effective stress for transport properties of inhomogeneous porous rock," J. Geophys. Res. **97**, 17409, https://doi.org/10.1029/92JB01593 (1992).
[30] B. Tully and Y. Ventikos, "Cerebral water transport using multiple-network poroelastic theory: Application to normal pressure hydrocephalus," J. Fluid Mech. **667**, 188 (2011).
[31] L. Asner, M. Hadjicharalambous, R. Chabiniok, D. Peressutti, E. Sammut, J. Wong, G. Carr-White, R. Razavi, A. King, and N. Smith, "Patient-specific modeling for left ventricular mechanics using data-driven boundary energies," Comput. Methods Appl. Mech. Eng. **314**, 269 (2017).
[32] G. B. Sands, D. A. Gerneke, D. A. Hooks, C. R. Green, B. H. Smaill, and I. J. Legrice, "Automated imaging of extended tissue volumes using confocal microscopy," Microsc. Res. Tech. **67**, 227 (2005).

16 January 2026 16:04:00

© Author(s) 2026

[33] M. Sankaranarayanan, L. P. Chua, D. N. Ghista, and Y. S. Tan, "Computational model of blood flow in the aorto-coronary bypass graft," BioMed. Eng. OnLine **4**, 14 (2005).

[34] R. J. Cerci, A. Arbab-Zadeh, R. T. George, J. M. Miller, A. L. Vavere, V. Mehra, K. Yoneyama, J. Texter, C. Foster, W. Guo, C. Cox, J. Brinker, M. Di Carli, and J. A. Lima, "Aligning coronary anatomy and myocardial perfusion territories: An algorithm for the CORE320 multicenter study," Circ: Cardiovasc. Imaging **5**, 587 (2012).

[35] E. B. Kesieme and K. G. Buchan, "Clinical anatomy of the coronary venous system and relevance to retrograde cardioplegia and cardiac electrophysiological interventions," Clin. Anat. **38**, 43 (2025).

[36] T. P. Van de Hoef, F. Nolte, R. Delewi, J. P. Henriques, J. A. Spaan, J. G. Tijssen, M. Siebes, J. J. Wykrzykowska, G. W. Stone, and J. J. Piek, "Intracoronary hemodynamic effects of pressure-controlled intermittent coronary sinus occlusion (PICSO): Results from the first-in-man prepare PICSO study," J. Interventional Cardiol. **25**, 549 (2012).

[37] R. R. Bouchard, S. J. Hsu, M. L. Palmeri, N. C. Rouze, K. R. Nightingale, and G. E. Trahey, "Acoustic radiation force-driven assessment of myocardial elasticity using the displacement ratio rate (DRR) method," Ultrasound Med. Biol. **37**, 1087 (2011).

[38] J. Schulz-Menger, D. A. Bluemke, J. Bremerich, S. D. Flamm, M. A. Fogel, M. G. Friedrich, R. J. Kim, F. von Knobelsdorff-Brenkenhoff, C. M. Kramer, D. J. Pennell, S. Plein, and E. Nagel, "Standardized image interpretation and post processing in cardiovascular magnetic resonance: Society for cardiovascular magnetic resonance (SCMR) board of trustees task force on standardized post processing," J. Cardiovasc. Magn. Reson. **15**, 35 (2013).

[39] T. A. Fairbairn, M. Motwani, A. N. Mather, J. D. Biglands, A. M. Larghat, A. Radjenovic, J. P. Greenwood, and S. Plein, "Cardiac MR imaging to measure myocardial blood flow response to the cold pressor test in healthy smokers and nonsmokers," Radiology **270**, 82 (2014).

[40] R. K. Hughes, J. B. Augusto, K. Knott, R. Davies, H. Shiwani, A. Seraphim, J. W. Malcolmson, S. Khoury, G. Joy, S. Mohiddin, L. R. Lopes, W. J. McKenna, P. Kellman, H. Xue, M. Tome, S. Sharma, G. Captur, and J. C. Moon, "Apical ischemia is a universal feature of apical hypertrophic cardiomyopathy," Circ: Cardiovasc. Imaging **16**, e014907 (2023).

[41] D. Likhite, G. Adluru, N. Hu, C. McGann, and E. DiBella, "Quantification of myocardial perfusion with self-gated cardiovascular magnetic resonance," J. Cardiovasc. Magn. Reson. **17**, 14 (2015).

[42] R. Catania, S. Quinn, A. A. Rahsepar, T. Agirlar Trabzonlu, J. B. Bisen, K. Chow, D. C. Lee, R. Avery, P. Kellman, and B. D. Allen, "Quantitative stress first-pass perfusion cardiac MRI: State of the art," Radiographics **45**, e240115 (2025).

[43] G. Di Gioia, J. A. Melin, and B. De Bruyne, "Coronary autoregulatory plateau in humans," J. Am. Coll. Cardiol. **76**, 1270 (2020).

[44] K. May-Newman, J. H. Omens, R. S. Pavelec, and A. D. McCulloch, "Three-dimensional transmural mechanical interaction between the coronary vasculature and passive myocardium in the dog," Circ. Res. **74**, 1166 (1994).

[45] A. D. McCulloch, P. J. Hunter, and B. H. Smaill, "Mechanical effects of coronary perfusion in the passive canine left ventricle," Am. J. Physiol. Heart Circ. Physiol. **262**, H523 (1992).

[46] M. Dewey, M. Siebes, M. Kachelriess, K. F. Kofoed, P. Maurovich-Horvat, K. Nikolaou, W. Bai, A. Kofler, R. Manka, S. Kozerke, A. Chiribiri, T. Schaeffter, F. Michallek, F. Bengel, S. Nekolla, P. Knaapen, M. Lubberink, R. Senior, M. X. Tang, J. J. Piek, T. van de Hoef, J. Martens, and L. Schreiber on behalf of the Quantitative Cardiac Imaging Study Group, "Clinical quantitative cardiac imaging for the assessment of myocardial ischaemia," Nat. Rev. Cardiol. **17**, 427 (2020).

[47] W. Yang, F. Zhang, H. Tang, X. Shao, J. Wang, X. Wang, X. Shao, W. Xin, L. Yang, W. Zhou, and Y. Wang, "Summed thickening score by myocardial perfusion imaging: A risk factor of left ventricular remodeling in patients with myocardial infarction," J. Interventional Cardiol. **25**, 742 (2018).

[48] S. E. Petersen, M. Jerosch-Herold, L. E. Hudsmith, M. D. Robson, J. M. Francis, H. A. Doll, J. B. Selvanayagam, S. Neubauer, and H. Watkins, "Evidence for microvascular dysfunction in hypertrophic cardiomyopathy," Circulation **115**, 2418 (2007).

[49] O. M. Muehling, N. M. Wilke, P. Panse, M. Jerosch-Herold, B. V. Wilson, R. F. Wilson, and L. W. Miller, "Reduced myocardial perfusion reserve and transmural perfusion gradient in heart transplant arteriopathy assessed by magnetic resonance imaging," J. Am. Coll. Cardiol. **42**, 1054 (2003).

[50] C. S. Hayward, W. V. Kalnins, and R. P. Kelly, "Gender-related differences in left ventricular chamber function," Cardiovasc. Res. **49**, 340 (2001).

[51] J. E. Davies, Z. I. Whinnett, D. P. Francis, C. H. Manisty, J. Aguado-Sierra, K. Willson, R. A. Foale, I. S. Malik, A. D. Hughes, K. H. Parker, and J. Mayet, "Evidence of a dominant backward-propagating "suction" wave responsible for diastolic coronary filling in humans, attenuated in left ventricular hypertrophy," Circulation **113**, 1768 (2006).

[52] R. Chabiniok, V. Y. Wang, M. Hadjicharalambous, L. Asner, J. Lee, M. Sermesant, E. Kuhl, A. A. Young, P. Moireau, M. P. Nash, D. Chapelle, and D. A. Nordsletten, "Multiphysics and multiscale modelling, data-model fusion and integration of organ physiology in the clinic: Ventricular cardiac mechanics," Interface Focus **6**, 20150083 (2016).

[53] N. Kaneko, R. Matsuda, M. Toda, and K. Shimamoto, "Three-dimensional reconstruction of the human capillary network and the intramyocardial micronecrosis," Am. J. Physiol. Heart Circ. Physiol. **300**, H754 (2011).

16 January 2026 16:04:00

© Author(s) 2026